Research Paper
Computational Methods for Differential Equations
http://cmde.tabrizu.ac.ir
Vol. 13, No. 3, 2025, pp. 783-801
DOI:10.22034/CMDE.2024.61485.2653

A study on the fractional Ebola virus model by the semi-analytic and numerical approach

Sachin Kelagere Narayana, Suguntha Devi Kannadasan*, and Kumbinarasaiah Srinivasa
Department of Mathematics, Bangalore University, Bengaluru-560056, India.

Abstract

In this study, an Ebola virus model involving fractional derivatives in the Caputo sense is considered and studied through three different techniques called the homotopy analysis method (HAM), the Haar wavelet method (HWM), and the Runge-Kutta method (RKM). The HAM is a semi-analytical approach proposed for solving fractional-order nonlinear systems of ordinary differential equations (ODEs), the Haar wavelet technique (HWT) is a numerical approach for both fractional and integer order, and the RKM is a numerical method used to solve the system of ODEs. We have drawn a semi-analytical solution in terms of a series of polynomials and numerical solutions for the model. First, we solved the model through the HAM by choosing the preferred control parameter. Secondly, the HWT is considered; through this technique, the operational matrix of integration is used to convert the given fractional differential equations (FDEs) into a set of algebraic equation systems, and then the RKM is applied. The model is studied through all three methods, and the solutions are juxtaposed with ND Solver solutions. The nature of the model is analyzed with different parameters, and the calculations are performed using Scilab and Mathematica software. The obtained results are expressed in graphs and tables. Convergence analysis has been discussed in terms of theorems.

Keywords. Fractional calculus, Ebola virus model, Homotopy analysis method, Haar wavelet.
1991 Mathematics Subject Classification. 26A33, 34A08, 65H20, 65T60.

1. Introduction

Ebola virus disease (EVD) is brought on by the Ebola virus, which was initially identified in 1976 in nations around the Ebola River in West Africa. It is considered to be the most deadly viral disease. Ebola is the worst infection because it may be transmitted from person to person via direct contact with infected persons. Humans can contract it from infected animals, primarily fruit bats, monkeys, porcupines, gorillas, and chimpanzees, through direct contact with their body fluids. The specific origin of the Ebola virus has yet to be identified, even though bats and other animals, including monkeys, gorillas, and chimpanzees, are thought to be the source of this particular virus. The Ebola virus has a high mortality rate and produces severe viral hemorrhagic fever. There are five species of Ebola viruses in the genus Ebola virus; four of these species cause EVD in humans, whereas the fifth species solely infects nonhuman primates (NHPs) [21]. Several mathematical models have been put out to examine how the West African Ebola outbreak in 2014 spread. It is known that statistical techniques and mathematical models are used to project the development of the disease; these days, a lot of researchers are focusing on the modeling and analysis of various problems in the field of biomathematical sciences, which presents a variety of data sets about a biological phenomenon like the Ebola virus, the distribution of bacterial cells, viruses, and the nervous system.

Numerous biological systems have been effectively and thoroughly modeled using ODEs. ODE-based models may be used to investigate the resilience and fragility of a system, identify limit cycles, and aid in studying bifurcation behavior, among other applications in system dynamics research. Since FDEs are determined to be the best representation of chemical processes, science, and physical models, fractional calculus (FC) has been extensively applied in these fields.

Received: 02 May 2024 ; Accepted: 31 July 2024.
∗ Corresponding author. Email: suganthadevik77@gmail.com.

In recent decades, FC has become more significant in various engineering and applied scientific domains, including fluid mechanics, viscoelasticity, convection, economics, electric transmission, and modeling of speech signals.

Researchers in several branches of science, mathematics, and engineering have paid close attention to mathematical models containing fractional derivatives in recent years. Over the last several decades, fractional calculus has grown in popularity and significance for many scholars due to its extensive applications in various scientific and technical fields. Additionally, fractional derivatives have been used to describe several complicated biological systems; physical and technical issues with viscoelasticity, physics, and fluid mechanics have led to more advancements in some fractional operators for precise modeling of the memory effects while dealing with various disorders.

This work proposes numerical and semi-analytical techniques to solve the following fractional-order Ebola virus epidemiological model:

$$\begin{cases} \mathscr{D}^{\alpha}\mathscr{S}(t) = -a\mathscr{S}(t)\mathscr{I}(t) + b\mathscr{R}(t) - cN, \\ \mathscr{D}^{\alpha}\mathscr{I}(t) = a\mathscr{S}(t)\mathscr{I}(t) - d\mathscr{I}(t) - e\mathscr{I}(t), \\ \mathscr{D}^{\alpha}\mathscr{R}(t) = e\mathscr{I}(t) - b\mathscr{R}(t), \\ \mathscr{D}^{\alpha}\mathscr{Z}(t) = d\mathscr{I}(t) + cN, \end{cases} \tag{1.1}$$

with initial conditions

$$\mathscr{S}(0) = \mathscr{S}_0, \quad \mathscr{I}(0) = \mathscr{I}_0, \quad \mathscr{R}(0) = \mathscr{R}_0, \quad \mathscr{Z}(0) = \mathscr{Z}_0.$$

A method that yields the analytic solution after some iterations is called a semi-analytical method. Here, we considered one of the semi-analytic methods used to solve a system of FDEs called the HAM. The HAM creates a convergent series solution for nonlinear mathematical models by using the idea of the homotopy in the topology. It is possible by using a homotopy-Maclaurin series to handle the system's nonlinearities. In 1992, the HAM was created for the first time in Shanghai Jiaotong University by Liao Shijun for his Ph.D. thesis [14]. Then, in 1997, it was modified by adding an auxiliary parameter [15] C_0 ($\neq 0$) known as the convergence-control parameter [16]. A non-physical variable called the convergence control parameter offers an easy approach to confirming and enforcing the convergence of a solution series. It is unusual for the HAM to naturally demonstrate the convergence in analytical and semi-analytic techniques to nonlinear differential equations. First, unlike other series expansion techniques, the HAM does not rely on either small or large physical factors directly, which allows it to apply to both strongly and weakly nonlinear problems, overcoming some inherent limitations of the standard perturbation methods. Second, the HAM unifies the Adomian decomposition method (ADM), the delta-expansion method, the homotopy perturbation method, and the Lyapunov artificial small parameter approach [13, 23]. Strong solution convergence over the broader region and parameter domains is frequently possible due to the method's enhanced generality. Third, the HAM offers super flexibility in the solution's representation and in the method by which it is expressly achieved. The basis functions of the intended solution and the related auxiliary linear operator of the homotopy can both be chosen with a significant degree of freedom. Finally, the HAM is a straightforward method that guarantees the convergence of the solution series, in contrast to the other analytical approximation methods.

We found several methods are used to analyze fractional EVD models, such as the Adam-Bashforth method [5], the Sinc-Legendre collocation method [4], the Chebyshev spectra collocation method [28], Lagrange polynomial functions [27], the fractional Adam-Bashforth method [2, 8], the homotopy decomposition method [1], the Runge Kutta IV and V order method [20], the optimal perturbation iteration method [29], the computational method based on iterative scheme [25], different fractional methods of the SIZR model [7], and the SIR model [6, 22].

Here, we applied the HWT to solve the model. When representing data or other functions, wavelets are mathematical functions that meet specific criteria. Since Joseph Fourier realized that sines and cosines could be superposed to describe other functions in the early 1800s, approximation utilizing the superposition of functions has been used. In the 1980s and 1990s, wavelets were created as an alternative to Fourier analysis of signals. Jean Morlet, Baroness Ingrid Daubechies, Alex Grossman, Palle Jorgensen, Yves Meyer, Ronald Coifman, Alfred Haar, and Stephane Mallat were a few key players in this invention. Yet, the scale at which we examine the data has a specific significance in wavelet analysis. Different scales or resolutions of data are processed by wavelet algorithms. Wavelet transforms are extremely helpful for signal analysis, compression, and de-noising. Fourier analysis is impoverished at approximating sharp spikes when investigating its solutions; however, we can employ approximation functions that are tidily contained in finite domains in appreciations of wavelet analysis. For estimating data with sharp discontinuities, wavelets work well. Compared to other methods [9, 11], the wavelet approach gives better outcomes. Numerical methods based on wavelets are effective for solving FDEs [26]. The Haar wavelets are compactly supported, and orthogonal with multi-resolution analysis [12]. According to our knowledge, we could not find any work on applying the HAM and the HWT to the fractional Ebola model, so we have solved the above model through the HAM and the HWT.

This paper is arranged as described as follows. Preliminaries of the Haar wavelets and their operational integration matrix are covered in section 2. The HAM and the HWT, which are employed to solve the model, are explained in section 3. A convergence analysis of the HAM and the HWT is drawn in section 4. Implementation of the methods to the model is discussed in section 5. The conclusion is outlined in section 6.

2. Priliminaries

In this section, we present the fundamentals of the Haar wavelets and their operational integration matrix. First, we will review the definition of a wavelet.

A wavelet can be expressed as a real-valued function $\Psi(t)$ that satisfies the following conditions [24]:

$$\int_{-\infty}^{\infty} \Psi(t)dt = 0, \qquad \text{and} \qquad \int_{-\infty}^{\infty} |\Psi(t)|^2 dt = 1.$$

This means that $\Psi(t)$ is an oscillatory function having unit energy and zero mean. More precisely, wavelets are defined as

$$\Psi_{a,b}(t) = \frac{1}{\sqrt{a}}\Psi(\frac{t-b}{a}), \quad a \neq 0,\ b \in \mathbb{R},$$

where a and b, respectively, represent the dilation and translation. Consider an interval [A, B] $\subset \mathbb{R}$, which is divided into m subintervals, having the interval size $\Delta t = \frac{B-A}{m}$. The i^{th} orthogonal set of Haar functions defined on the interval $[A, B]$ is defined as

$$h_i(t) = \begin{cases} 1, & \zeta_1(i) \leq t < \zeta_2(i), \\ -1, & \zeta_2(i) \leq t < \zeta_3(i), \\ 0, & otherwise, \end{cases} \tag{2.1}$$

where,

$$\zeta_1(i) = A + \frac{k-1}{2^j} m\Delta t,$$
$$\zeta_2(i) = A + \frac{k-(\frac{1}{2})}{2^j} m\Delta t,$$
$$\zeta_3(i) = A + \frac{k}{2^j} m\Delta t,$$

for $i = 1, 2, ..., m,\ m = 2^J$, and $J \in Z^+$ called the maximum level of resolution. Here k and j are the integer decomposition of the index i, that is, $i = k + 2^j - 1$, $0 \leq j < 1$, and $1 \leq k < 2^j + 1$. Eq. (2.1) is valid for $i \geq 2$; for $i = 1$ we have

$$h_i(t) = \begin{cases} 1, & for \quad x \in [A, B], \\ 0, & otherwise. \end{cases} \tag{2.2}$$

Now, we indicate how the operational integration matrix of the Haar wavelets can be obtained. For the integration of the general order α, the Haar wavelet operational matrix Q^α is provided by

$$Q^\alpha H_m(t) = J^\alpha H_m(t) = [J^\alpha h_0(t), J^\alpha h_1(t), J^\alpha h_2(t), ..., J^\alpha h_{m-1}(t)],$$

$$Q^\alpha H_m(t) = [Qh_0(t), Qh_1(t), Qh_2(t), ..., Qh_{m-1}(t)], \tag{2.3}$$

where

$$Qh_i(t) = \begin{cases} 0, & A \leq t < \zeta_1(i), \\ \Phi_1, & \zeta_1(i) \leq t < \zeta_2(i), \\ \Phi_2, & \zeta_2(i) \leq t < \zeta_3(i), \\ \Phi_3, & \zeta_2(i) \leq t < B, \end{cases} \tag{2.4}$$

where

$$\begin{aligned} \Phi_1 &= \frac{(t-\zeta_1(i))^\alpha}{\Gamma(\alpha+1)}, \\ \Phi_2 &= \frac{(t-\zeta_1(i))^\alpha}{\Gamma(\alpha+1)} - 2\frac{(t-\zeta_2(i))^\alpha}{\Gamma(\alpha+1)}, \\ \phi_3 &= \frac{(t-\zeta_1(i))^\alpha}{\Gamma(\alpha+1)} - 2\frac{(t-\zeta_2(i))^\alpha}{\Gamma(\alpha+1)} + \frac{(t-\zeta_3(i))^\alpha}{\Gamma(\alpha+1)}. \end{aligned}$$

Eq. (2.4) is valid for $i \geq 1$. For $i = 0$, we have

$$Qh_0(t) = \begin{cases} \frac{t^\alpha}{\Gamma(\alpha+1)}, & t \in [A, B], \\ 0, & otherwise. \end{cases}$$

For instance, if $\alpha \in \mathbb{R}$, we construct an operational matrix for various α and J values in the next cases.

Case 1. For $\alpha = 1$ and $J = 3$, the operational matrix is obtained as follows:

$$Q^1 H_m(t) = \begin{bmatrix} 0.0625 & 0.1875 & 0.3125 & 0.4375 & 0.5625 & 0.6875 & 0.8125 & 0.9375 \\ 0.0625 & 0.1875 & 0.3125 & 0..4375 & 0.4375 & 0.3125 & 0.1875 & 0.0625 \\ 0.0625 & 0.1875 & 0.1875 & 0.0625 & 0 & 0 & 0 & 0 \\ 0 & 0 & 0 & 0 & 0.0625 & 0.1875 & 0.1875 & 0.0625 \\ 0.0625 & 0.0625 & 0 & 0 & 0 & 0 & 0 & 0 \\ 0 & 0 & 0.0625 & 0.0625 & 0 & 0 & 0 & 0 \\ 0 & 0 & 0 & 0 & 0.0625 & 0.0625 & 0 & 0 \\ 0 & 0 & 0 & 0 & 0 & 0 & 0.0625 & 0.0625 \end{bmatrix}. \tag{2.5}$$

Case 2. Considering $\alpha = 2$ and $J = 3$, the operational matrix is achieved as

$$Q^2 H_m(t) = \begin{bmatrix} 0.00195313 & 0.0175781 & 0.0488281 & 0.0957031 & 0.158203 & 0.236328 & 0.330078 & 0.439453 \\ 0.00195313 & 0.0175781 & 0.0488281 & 0.0957031 & 0.154297 & 0.201172 & 0.232422 & 0.248047 \\ 0.00195313 & 0.0175781 & 0.0449219 & 0.0605469 & 0.0625 & 0.0625 & 0.0625 & 0.0625 \\ 0 & 0 & 0 & 0 & 0.00195313 & 0.0175781 & 0.0449219 & 0.0605469 \\ 0.00195313 & 0.0136719 & 0.015625 & 0.015625 & 0.015625 & 0.015625 & 0.015625 & 0.015625 \\ 0 & 0 & 0.00195313 & 0.0136719 & 0.015625 & 0.015625 & 0.015625 & 0.015625 \\ 0 & 0 & 0 & 0 & 0.00195313 & 0.0136719 & 0.015625 & 0.015625 \\ 0 & 0 & 0 & 0 & 0 & 0 & 0.00195313 & 0.0136719 \end{bmatrix}.$$

Case 3. Similarly, we obtain the operational matrix for $\alpha = 1.5$ and $J = 3$ in the following equation:

$$Q^{1.5} H_m(t) = \begin{bmatrix} 0.0117539 & 0.0610753 & 0.131413 & 0.217686 & 0.317357 & 0.428818 & 0.550933 & 0.682843 \\ 0.0117539 & 0.0610753 & 0.131413 & 0.217686 & 0.293849 & 0.306667 & 0.288107 & 0.24747 \\ 0.0117539 & 0.0610753 & 0.107905 & 0.0955356 & 0.0662843 & 0.0545208 & 0.047633 & 0.0428933 \\ 0 & 0 & 0 & 0 & 0.0117539 & 0.0610753 & 0.107905 & 0.0955356 \\ 0.117539 & 0.0375674 & 0.0210165 & 0.0159352 & 0.0133974 & 0.0117908 & 0.010654 & 0.00979445 \\ 0 & 0 & 0.117539 & 0.0375674 & 0.0210165 & 0.0159352 & 0.0133974 & 0.0117908 \\ 0 & 0 & 0 & 0 & 0.117539 & 0.0375674 & 0.0210165 & 0.0159352 \\ 0 & 0 & 0 & 0 & 0 & 0 & 0.117539 & 0.0375674 \end{bmatrix}.$$

In a similar way, we can develop the operational matrix of the Haar wavelets for distinct α values as per our requirements.

3. Method of Solution

This section describes the HAM and HWT that are used to solve the model. The implementation of the HWT for the specified fractional model is also discussed further below.

3.1. **The homotopy analysis method.** Consider the system of nonlinear FDEs with different physical conditions [30]

$$\mathscr{D}^{\alpha}[y_i(t)] = g_i(t, y_1, y_2, ..., y_n), \qquad i = 1, 2, 3, ..., n, \quad 0 < \alpha \leq 1, \quad t \geq 0, \tag{3.1}$$

subject to the conditions:

$$y_i = a_i, \qquad i = 1, 2, 3, ..., n, \tag{3.2}$$

where $\mathscr{D}^{\alpha}$ represents the differential operator and $y_i(t)$ is the function to be determined.

The zeroth-order deformation equation. Let $y_{i_0}(t)$, $i = 1, 2, 3, ..., n$, be the initial approximation to the actual solution of (3.1). Liao constructed zeroth deformation equations taking the auxiliary functions $\mathscr{H}$(t) ($\neq 0$) and auxiliary parameter $\hbar$ ($\neq 0$) as [10]

$$(1 - q)\mathscr{L}_i[\phi_i(t; q) - y_{i_0}(t)] = q\hbar\mathscr{H}(t)\mathscr{N}_i[\phi_i(t; q)], \quad i = 1, 2, 3, ..., n, \tag{3.3}$$

subject to the following conditions:

$$\phi_i(0; q) = a_i, \quad i = 1, 2, 3, ..., n, \tag{3.4}$$

where $\phi_i(t; q)$ are unknown functions and $\mathscr{L}_i$ are the linear operators.

When $q = 0$, Eq. (3.3) becomes $\phi_i(t; 0) = y_{i_0}(t)$, and at q=1, it changes to $\phi_i(t; 1) = y_i(t)$. So as the q varies from 0 to 1, the function $\phi_i(t; q)$ varies from the initial approximation $y_{i_0}(t)$ to the actual solution $y_i(t)$, $i = 1, 2, 3, ..., n$. Defining the m^{th} order deformation derivatives," with "The m^{th} order deformation derivative is defined as follows:

$$y_{i_m}(t) = \frac{1}{m!}\frac{\partial^m \phi_i(t; q)}{\partial q^m}, \quad i = 1, 2, 3, ..., n. \tag{3.5}$$

Expanding $\phi_i(t; q)$ using the Taylor series with respect to q, for $i = 1, 2, 3, ..., n$, we get

$$\phi_i(t; q) = y_{i_0}(t) + \sum_{m=1}^{\infty} y_{i_m}(t)q^m, \quad i = 1, 2, 3, ..., n. \tag{3.6}$$

As we know, at $q = 1$, $\phi_i(t; q)$ becomes the required solution. Therefore, Eq. (3.6) at q=1 turns into

$$\phi_i(t; 1) = y_i(t) = y_{i_0}(t) + \sum_{m=1}^{\infty} y_{i_m}(t), \quad i = 1, 2, 3, ..., n. \tag{3.7}$$

Similarly, the equation for m^{th} order deformation is provided by

$$\mathscr{L}[y_{i_m}(t) - \chi_m y_{i_{m-1}}(t)] = \hbar\mathscr{H}(t)R_{i,m}(y_{i_{m-1}}(t)), \quad i = 1, 2, 3, ..., n, \tag{3.8}$$

where

$$\chi_m = \begin{cases} 0, & if \quad m \leq 1, \\ 1, & otherwise, \end{cases} \tag{3.9}$$

and

$$R_{i,m}(y_{i_{m-1}}(t))) = \frac{1}{(m-1)!}\frac{\partial^{m-1}[\mathscr{N}[\phi_i(t; q)]]}{\partial q^{m-1}}, \quad i = 1, 2, 3, ..., n. \tag{3.10}$$

Thus, $y_{i_1}(t)$, $y_{i_2}(t)$, $y_{i_3}(t)$, and so on can be obtained from solving Eq. (3.8). The m^{th} order approximation of $y_i(t)$ [16–18] is given by

$$y_i(t) = \sum_{m=0}^{m} y_{i_m}(t). \tag{3.11}$$

As a result, Eq. (3.11) is the semi-analytical solution of (3.1).

It is worth noting that the approach described above can be used to solve fractional differential equations. However, in a differential equation of non-fractional order, the inverse of the linear operator will be integration, whereas in a differential equation of fractional order, it will be a fractional integration

3.2. **The Haar wavelet technique.** Consider the following system of n differential equations:

$$\begin{cases} y_1^{'}(x) = f_1(t, y_1(x), ..., y_n(x)), \\ y_2^{'}(x) = f_2(t, y_1(x), ..., y_n(x)), \\ \vdots \\ y_n^{'}(x) = f_n(t, y_1(x), ..., y_n(x)), \end{cases} \tag{3.12}$$

with initial conditions $y_k(0)$=α_k, where $k = 1, 2, ..., n$. To find the Haar wavelet solution of this system of ODEs. We find the collocation points as

$$x_l = 0.5(\tilde{x}_{l-1} + \tilde{x}_l), \qquad l = 1, 2, ..., 2M,$$

where

$$\tilde{x}_l = a + l\Delta x, \qquad\qquad l = 0, 1, 2, ..., 2M.$$

Now, the Haar wavelet approximation of (3.12) can be written as

$$y_k^{'}(x) = \sum_{i=1}^{2M} a_i^k h_i(x). \tag{3.13}$$

Integrating (3.13) with respect to x from 0 to x, we get

$$y_k(x) = y_k(0) + \sum_{1=1}^{2M} a_i^k P_{1,i}(x),$$

$$y_k(x) = \alpha_k + \sum_{1=1}^{2M} a_i^k P_{1,i}(x), \tag{3.14}$$

where $P_{1,i}$ is the first operational matrix of integration. Substituting the Eqs. (3.13) and (3.14) in (3.12) and replacing x by x_l, then the diabetes model reduces to a system of nonlinear algebraic equations as follows:

$$\begin{cases} F_1(a_1^1, a_2^1, ..., a_{2M}^1, a_1^2, a_2^2, ..., a_{2M}^2, ..., a_1^n, a_2^n, ..., a_{2M}^n) = 0, \\ F_2(a_1^1, a_2^1, ..., a_{2M}^1, a_1^2, a_2^2, ..., a_{2M}^2, ..., a_1^n, a_2^n, ..., a_{2M}^n) = 0, \\ \qquad\qquad \vdots \\ F_n(a_1^1, a_2^1, ..., a_{2M}^1, a_1^2, a_2^2, ..., a_{2M}^2, ..., a_1^n, a_2^n, ..., a_{2M}^n) = 0. \end{cases} \tag{3.15}$$

In order to determine the values of the Haar coefficients a_i^k, the Newton-Raphson technique was taken into consideration. In the event when a_i^k is the initial guess and the slope intercept point is a_{i+1}^k, the Taylor series expansion of (3.15) may be expressed as

$$F_{1,i+1} = F_{1,i} + (a_{1,i+1}^k - a_{1,i}^k)\frac{\partial F_{1,i}}{\partial a_1^k} + (a_{2,i+1}^k - a_{2,i}^k)\frac{\partial F_{1,i}}{\partial a_2^k} +, ..., +(a_{2M,i+1}^k - a_{2M,i}^k)\frac{\partial F_{1,i}}{\partial a_{2M}^k}, \tag{3.16}$$

where k=1,2,3,...,n. Applying the Taylor expansion similarly for $F_2, F_3, F_4, ..., F_n$, and generalizing for n equations, we get

$$\frac{\partial F_{k,i}}{\partial a_1^k} a_{1,i+1}^k + \frac{\partial F_{k,i}}{\partial a_2^k} a_{2,i+1}^k +, ..., +\frac{\partial F_{k,i}}{\partial a_{2M}^k} a_{2M,i+1}^k = -F_{k,i} + a_{1,i}^k \frac{\partial F_{k,i}}{\partial a_1^k} + a_{2,i}^k \frac{\partial F_{k,i}}{\partial a_2^k} +, ..., +a_{2M,i}^k \frac{\partial F_{k,i}}{\partial a_{2M}^k}. \tag{3.17}$$

The equations in (3.15) are represented by the first subscript k, and the function value at the current value (i) or the next value $(i+1)$ is indicated by the second subscript. Eq. (3.17) can be represented in matrix notation as

$$[J][a_{i+1}^k] = -[F] + [J][a_i^k], \tag{3.18}$$

where the partial derivatives evaluated at i are written as the Jacobian matrix consisting of partial derivatives

$$[J] = \begin{bmatrix} \frac{\partial F_{1,i}}{\partial a_1^k} & \frac{\partial F_{1,i}}{\partial a_2^k} & \cdots & \frac{\partial F_{1,i}}{\partial a_{2M}^k} \\ \frac{\partial F_{2,i}}{\partial a_1^k} & \frac{\partial F_{2,i}}{\partial a_2^k} & \cdots & \frac{\partial F_{2,i}}{\partial a_{2M}^k} \\ \vdots & & \cdots & \vdots \\ \frac{\partial F_{n,i}}{\partial a_1^k} & \frac{\partial F_{n,i}}{\partial a_2^k} & \cdots & \frac{\partial F_{n,i}}{\partial a_{2M}^k} \end{bmatrix}. \tag{3.19}$$

The initial and final values are expressed in vector form as

$$[a_i^k]^T = \begin{bmatrix} a_{1,i}^k & a_{2,i}^k & \cdots & a_{2M,i}^k \end{bmatrix}, \; [a_{i+1}^k]^T = \begin{bmatrix} a_{1,i+1}^k & a_{2,i+1}^k & \cdots & a_{n,i+1}^k \end{bmatrix}, \text{ and } [F]^T = \begin{bmatrix} F_{1,i} & F_{2,i} & \cdots & F_{n,i} \end{bmatrix}.$$

Multiplying the inverse of the Jacobian matrix to (3.18) yields

$$[a_{i+1}^k] = [a_i^k] - [J]^{-1}[F]. \tag{3.20}$$

From (3.20), we get the Haar wavelet coefficients $a_i^k s$. Using $a_i^k s$ in Eq. (3.14), we get the desired solution of the diabetes model (3.12).

3.2.1. **Implementing the HWT for the fractional model.** Consider the general form of the fractional model

$$\begin{cases} D^\alpha y_1(t) = f_1(t, y_1(t), ..., y_n(t)), \\ D^\alpha y_2(t) = f_2(t, y_1(t), ..., y_n(t)), \\ \qquad\qquad \vdots \\ D^\alpha y_n(t) = f_n(t, y_1(t), ..., y_n(t)), \end{cases} \tag{3.21}$$

with initial conditions $y_i(t) = \beta_k, i = 1, 2, ..., n$, where $\mathscr{D}^\alpha$ represents the Caputo differential operator. The Haar wavelet approximation is given as

$$\frac{dy_k(t)}{dt} = \sum_{i=1}^{m} a_i^k h_m(t), \tag{3.22}$$

integrating the above equation with respect to t from 0 to t, we get

$$y_k(t) = \beta_k + \sum_{i=1}^{m} a_i^k Q^1 h_m(t), \quad \text{where} \quad 1 \le k \le n, \tag{3.23}$$

where $Q^1 H_m(t)$ is the first-order operational matrix of integration. Fractionally differentiating (3.23) with respect to t of order α, where $\alpha \in (0, 1)$, yields

$$\frac{d^\alpha y_k(t)}{dt^\alpha} = \frac{d^\alpha}{dt^\alpha}(\beta_k) + \sum_{i=1}^{m} a_i^k Q^{1-\alpha} H_m(t). \tag{3.24}$$

Substituting (3.22), (3.23), and (3.24) in (3.21) and replacing t by collocation points t_l given in section 3.2. Eq. (3.21) reduces to a system of nonlinear algebraic equations as follows:

$$\begin{cases} F_1(a_1^1, a_2^1, ..., a_m^1, a_1^2, a_2^2, ..., a_m^2, ..., a_1^n, a_2^n, ..., a_m^n) = 0, \\ F_2(a_1^1, a_2^1, ..., a_m^1, a_1^2, a_2^2, ..., a_m^2, ..., a_1^n, a_2^n, ..., a_m^n) = 0, \\ \qquad \vdots \\ F_n(a_1^1, a_2^1, ..., a_m^1, a_1^2, a_2^2, ..., a_m^2, ..., a_1^n, a_2^n, ..., a_m^n) = 0. \end{cases} \tag{3.25}$$

By which we find the values of Haar coefficients a_i^k's with the help of the Newton-Raphson method as follows: If the initial guess of the root is a_i^k and a_{i+1}^k is the point at which the slope intercepts, then the Taylor series expansion of (3.25) can be written as

$$F_{1,i+1} = F_{1,i} + (a_{1,i+1}^k - a_{1,i}^k)\frac{\partial F_{1,i}}{\partial a_1^k} + (a_{2,i+1}^k - a_{2,i}^k)\frac{\partial F_{1,i}}{\partial a_2^k} +, ..., +(a_{m,i+1}^k - a_{m,i}^k)\frac{\partial F_{1,i}}{\partial a_m^k}, \tag{3.26}$$

where k=1,2,3,...,n. Applying the Taylor expansion similarly for $F_2, F_3, F_4, ..., F_n$, and generalizing for n equations, we get

$$\frac{\partial F_{k,i}}{\partial a_1^k}a_{1,i+1}^k + \frac{\partial F_{k,i}}{\partial a_2^k}a_{2,i+1}^k +, ..., +\frac{\partial F_{k,i}}{\partial a_m^k}a_{m,i+1}^k = -F_{k,i} + a_{1,i}^k\frac{\partial F_{k,i}}{\partial a_1^k} + a_{2,i}^k\frac{\partial F_{k,i}}{\partial a_2^k} +, ..., +a_{m,i}^k\frac{\partial F_{k,i}}{\partial a_m^k}. \tag{3.27}$$

The first subscript k identifies the equation or unknown function, while the second subscript indicates the iteration step, either the current value (i) or the next value ($i+1$). Eq. (3.27) can be represented in matrix notation as

$$[J][a_{i+1}^k] = -[F] + [J][a_i^k], \tag{3.28}$$

where the partial derivatives evaluated at i are written as the Jacobian matrix consisting of partial derivatives

$$[J] = \begin{bmatrix} \frac{\partial F_{1,i}}{\partial a_1^k} & \frac{\partial F_{1,i}}{\partial a_2^k} & \cdots & \frac{\partial F_{1,i}}{\partial a_m^k} \\ \frac{\partial F_{2,i}}{\partial a_1^k} & \frac{\partial F_{2,i}}{\partial a_2^k} & \cdots & \frac{\partial F_{2,i}}{\partial a_m^k} \\ \vdots & & \cdots & \vdots \\ \frac{\partial F_{n,i}}{\partial a_1^k} & \frac{\partial F_{n,i}}{\partial a_2^k} & \cdots & \frac{\partial F_{n,i}}{\partial a_m^k} \end{bmatrix}.$$

The initial and final values are expressed in vector form as

$$[a_i^k]^T = \begin{bmatrix} a_{1,i}^k & a_{2,i}^k & \cdots & a_{m,i}^k \end{bmatrix},$$

$$[a_{i+1}^k]^T = \begin{bmatrix} a_{1,i+1}^k & a_{2,i+1}^k & \cdots & a_{n,i+1}^k \end{bmatrix},$$

and

$$[F]^T = \begin{bmatrix} F_{1,i} & F_{2,i} & \cdots & F_{n,i} \end{bmatrix}.$$

Multiplying the inverse of the Jacobian matrix to (3.28) results in

$$[a_{i+1}^k] = [a_i^k] - [J]^{-1}[F]. \tag{3.29}$$

From (3.29) we get the Haar wavelet coefficients $a_i^k s$. Using $a_i^k s$ in Eq. (3.23), we get the desired solution of the fractional model (3.21).

4. Convergence Analysis

Theorem 4.1. *As long as the series $y_0(t) + \sum_{m=1}^{\infty} y_m(t)$ converges, where $y_m(t)$ is governed by the higher-order deformation equation number χ_m given by (3.9), it must be the exact solution [16].*

Theorem 4.2. *Let $\phi_0, \phi_1, \phi_2, ...$ be the solution components of a given equation. The seris solution $\sum_{k=0}^{\infty} \phi_k(t)$ converges if $\exists\ 0 < \gamma < 1$ such that $||\phi_{k+1}|| \leq \gamma||\phi_k||$, $\forall\ k \geq k_0$ for some $k_0 \in \mathbb{N}$ [19].*

Theorem 4.3. *Assume that the series solution $\sum_{k=0}^{\infty} \phi_k(t)$ is convergent to the solution $y(t)$; if the truncation series $\sum_{k=0}^{m} \phi_k(t)$ is used as an approximation to the solution $y(t)$, then the maximum absolute truncation error is estimated as $||y(t) - \sum_{k=0}^{m} \phi_k(t)|| \leq \frac{1}{1-\gamma}\ \gamma^{m+1}\ ||\phi_0(t)||$ [19].*

Theorem 4.4. *Suppose that the functions $D_*^{\alpha} u_k(t)$ obtained by using Haar wavelets are the approximation of $D_*^{\alpha} u(t)$; then we have an exact upper bound as follows:*

$$||D_*^{\alpha} u(t) - D_*^{\alpha} u_k(t)||_E \leq \frac{M}{\Gamma(m-\alpha).(m-\alpha)} \frac{1}{[1-2^{2(\alpha-m)}]^{\frac{1}{2}}} \frac{1}{k^{m-\alpha}},$$

where

$$||u(t)||_E = (\int_0^1 u^2(t)dt)^{\frac{1}{2}}),$$

[3].

5. Solution of the Fractional Ebola Virus Model

Consider the described Ebola virus model as follows:

$$\begin{aligned}
&\mathscr{D}^\alpha \mathscr{S}(t) = -a\mathscr{S}(t)\mathscr{I}(t) + b\mathscr{R}(t) - cN,\\
&\mathscr{D}^\alpha \mathscr{I}(t) = a\mathscr{S}(t)\mathscr{I}(t) - d\mathscr{I}(t) - e\mathscr{I}(t),\\
&\mathscr{D}^\alpha \mathscr{R}(t) = e\mathscr{I}(t) - b\mathscr{R}(t),\\
&\mathscr{D}^\alpha \mathscr{Z}(t) = d\mathscr{I}(t) + cN,
\end{aligned} \tag{5.1}$$

with initial conditions

$$\mathscr{S}(0) = \mathscr{S}_0, \quad \mathscr{I}(0) = \mathscr{I}_0, \quad \mathscr{R}(0) = \mathscr{R}_0, \quad \mathscr{Z}(0) = \mathscr{Z}_0, \tag{5.2}$$

where, $\mathscr{S}(t)$, $\mathscr{I}(t)$, $\mathscr{R}(t)$, and $\mathscr{Z}(t)$ are susceptible, infect, recovery and dead populations, respectively, and the rates of infection, susceptibility, natural death, death from Ebola, and recovery, are denoted by a, b, c, d, and e, respectively, and N is the number of people in the population at a given time. Here we examine the functions $\mathscr{S}(t)$, $\mathscr{I}(t)$, $\mathscr{R}(t)$, and $\mathscr{Z}(t)$ taking the parameters $a = 0.001$, $b = 0.002$, $c = 0.01$, $d = 0.006$, $e = 0.004$, and $N = 72$. The initial data taken as $\mathscr{S}(0) = 70$, $\mathscr{I}(0) = 2$, $\mathscr{R}(0) = 0$, and $\mathscr{Z}(0) = 0$. Applying the above-presented HAM to (5.1) and (5.2). According to (3.3), the zeroth-order deformation is given by

$$\begin{aligned}
&(1-q)\mathscr{L}_1[\phi_1(t;q) - \mathscr{S}_0(t)] = q\hbar\mathscr{H}(t)[\mathscr{D}^\alpha\phi_1(t;q) + a\phi_1(t;q)\phi_2(t;q) - b\phi_3(t;q) + cN],\\
&(1-q)\mathscr{L}_2[\phi_2(t;q) - \mathscr{I}_0(t)] = q\hbar\mathscr{H}(t)[\mathscr{D}^\alpha\phi_2(t;q) - a\phi_1(t;q)\phi_2(t;q) + d\phi_2(t;q) + e\phi_2(t;q)],\\
&(1-q)\mathscr{L}_3[\phi_3(t;q) - \mathscr{R}_0(t)] = q\hbar\mathscr{H}(t)[\mathscr{D}^\alpha\phi_3(t;q) - e\phi_2(t;q) + b\phi_3(t;q)],\\
&(1-q)\mathscr{L}_4[\phi_4(t;q) - \mathscr{Z}_0(t)] = q\hbar\mathscr{H}(t)[\mathscr{D}^\alpha\phi_4(t;q) - d\phi_2(t;q) - cN].
\end{aligned} \tag{5.3}$$

According to the condition (5.2), we choose the initial approximations as $\mathscr{S}_0(t) = 70$, $\mathscr{I}_0(t) = 2$, $\mathscr{R}_0(t) = 0$ and $\mathscr{Z}_0(t) = 0$, taking the linear operator as $\mathscr{L}_i = \mathscr{D}^\alpha$ with $\mathscr{L}_i(C_i) = 0$, $i = 1, 2, 3, 4$. Where C_i, $i = 1, 2, 3, 4$, are integral constants with $\mathscr{H}(t) = 1$. Therefore, m^{th} order deformations are given by

$$\begin{aligned}
\mathscr{D}^\alpha[\mathscr{S}_m(t) - \chi_m\mathscr{S}_{m-1}(t)] &= \hbar R_{1,m}(\mathscr{S}_{m-1}(t)),\\
\mathscr{D}^\alpha[\mathscr{I}_m(t) - \chi_m\mathscr{I}_{m-1}(t)] &= \hbar R_{2,m}(\mathscr{I}_{m-1}(t)),\\
\mathscr{D}^\alpha[\mathscr{R}_m(t) - \chi_m\mathscr{R}_{m-1}(t)] &= \hbar R_{3,m}(\mathscr{R}_{m-1}(t)),\\
\mathscr{D}^\alpha[\mathscr{Z}_m(t) - \chi_m\mathscr{Z}_{m-1}(t)] &= \hbar R_{4,m}(\mathscr{Z}_{m-1}(t)),
\end{aligned} \tag{5.4}$$

subject to

$$\mathscr{S}_m(0) = 0, \qquad \mathscr{I}_m(0) = 0, \qquad \mathscr{R}_m(0) = 0, \qquad \mathscr{Z}_m(0) = 0, \qquad m \geq 1, \tag{5.5}$$

where

$$\begin{aligned}
&R_{1,m}(\mathscr{S}_{m-1}(t)) = \mathscr{D}^\alpha[\mathscr{S}_{m-1}(t)] + a\sum_{j=0}^{m-1}\mathscr{S}_j(t)\mathscr{I}_{m-1-j}(t) - b\mathscr{R}_{m-1}(t) + (1-\chi_m)cN,\\
&R_{2,m}(\mathscr{I}_{m-1}(t)) = \mathscr{D}^\alpha[\mathscr{I}_{m-1}(t)] - a\sum_{j=0}^{m-1}\mathscr{S}_j(t)\mathscr{I}_{m-1-j}(t) + d\mathscr{I}_{m-1}(t) + e\mathscr{I}_{m-1}(t),\\
&R_{3,m}(\mathscr{R}_{m-1}(t)) = \mathscr{D}^\alpha[\mathscr{R}_{m-1}(t)] - e\mathscr{I}_{m-1}(t) + b\mathscr{R}_{m-1}(t),\\
&R_{4,m}(\mathscr{Z}_{m-1}(t)) = \mathscr{D}^\alpha[\mathscr{Z}_{m-1}(t)] - d\mathscr{I}_{m-1}(t) - (1-\chi_m)cN.
\end{aligned} \tag{5.6}$$

Applying $\mathscr{J}^\alpha$, the inverse of $\mathscr{D}^\alpha$, on either side of (5.4), we get

$$\mathscr{S}_m(t) = \chi_m\mathscr{S}_{m-1}(t) + \hbar\mathscr{J}^\alpha[R_{1,m}(\mathscr{S}_{m-1}(t))] + C_1,$$

$$\begin{aligned}
&\mathscr{I}_m(t) = \chi_m \mathscr{I}_{m-1}(t) + \hbar \mathscr{J}^{\alpha}[R_{2,m}(\mathscr{I}_{m-1}(t))] + C_2,\\
&\mathscr{R}_m(t) = \chi_m \mathscr{R}_{m-1}(t) + \hbar \mathscr{J}^{\alpha}[R_{3,m}(\mathscr{R}_{m-1}(t))] + C_3,\\
&\mathscr{Z}_m(t) = \chi_m \mathscr{Z}_{m-1}(t) + \hbar \mathscr{J}^{\alpha}[R_{4,m}(\mathscr{Z}_{m-1}(t))] + C_4, \qquad m \geq 1.
\end{aligned} \tag{5.7}$$

C_1, C_2, C_3, and C_4 are calculated using (5.5).

The HAM series up to the first ten terms when $\alpha = 0.25$ and $h = -1$ is

$$\begin{aligned}
\mathscr{S}(t) = {} & 70 - 1.25772t^{0.25} - 0.00688763t^{0.5} - 0.000199874t^{0.75} - 1.81955 \times 10^{-6}t^{1}\\
& + 1.93713 \times 10^{-7}t^{1.25} + 1.39952 \times 10^{-8}t^{1.5} + 4.97401 \times 10^{-10}t^{1.75} + 5.86626 \times 10^{-12}t^{2}\\
& - 4.83915 \times 10^{-13}t^{2.25} - 3.75761 \times 10^{-14}t^{2.5},\\
\mathscr{I}(t) = {} & 2 + 0.132392t^{0.25} + 0.00555163t^{0.5} + 0.000147351t^{0.75} + 5.02804 \times 10^{-7}t^{1}\\
& - 1.97261 \times 10^{-7}t^{1.25} - 1.23124 \times 10^{-8}t^{1.5} - 3.96751 \times 10^{-10}t^{1.75} - 2.73935 \times 10^{-12}t^{2} +\\
& 5.03504 \times 10^{-13}t^{2.25} + 3.37036 \times 10^{-14}t^{2.5},\\
\mathscr{R}(t) = {} & 0.0088261t^{0.25} + 0.000523568t^{0.5} + 0.0000204034t^{0.75} + 5.04197 \times 10^{-7}t^{1}\\
& + 8.851 \times 10^{-10}t^{1.25} - 6.74013 \times 10^{-10}t^{1.5} - 3.95916 \times 10^{-11}t^{1.75} - 1.21256 \times 10^{-12}t^{2}\\
& - 6.69394 \times 10^{-15}t^{2.25} + 1.55517 \times 10^{-15}t^{2.5},\\
\mathscr{Z}(t) = {} & 1.1165t^{0.25} + 0.000812433t^{0.5} + 0.0000321197t^{0.75} + 8.12551 \times 10^{-7}t^{1}\\
& + 2.66268 \times 10^{-9}t^{1.25} - 1.00876 \times 10^{-9}t^{1.5} - 6.10587 \times 10^{-11}t^{1.75} - 1.91435 \times 10^{-12}t^{2}\\
& - 1.28948 \times 10^{-14}t^{2.25} + 2.31735 \times 10^{-15}t^{2.5}.
\end{aligned}$$

The HAM series up to the first ten terms when $\alpha = 0.5$ and $h = -1$ is

$$\begin{aligned}
\mathscr{S}(t) = {} & 70. - 1.28635t^{0.5} - 0.006104t^{1} - 0.000118167t^{1.5} + 1.12335 \times 10^{-6}t^{2}\\
& + 1.59407 \times 10^{-7}t^{2.5} + 4.94525 \times 10^{-9}t^{3} + 3.0227 \times 10^{-11}t^{3.5} - 3.57763 \times 10^{-12}t^{4}\\
& - 1.56023 \times 10^{-13}t^{4.5} - 2.16706 \times 10^{-15}t^{5},\\
\mathscr{I}(t) = {} & 2. + 0.135406t^{0.5} + 0.00492t^{1} + 0.0000818548t^{1.5} - 1.64866 \times 10^{-6}t^{2}\\
& - 1.49246 \times 10^{-7}t^{2.5} - 4.12324 \times 10^{-9}t^{3} - 9.29438 \times 10^{-12}t^{3.5} + 3.61476 \times 10^{-12}t^{4}\\
& + 1.39439 \times 10^{-13}t^{4.5} + 1.56463 \times 10^{-15}t^{5},\\
\mathscr{R}(t) = {} & 0.00902703t^{0.5} + 0.000464t^{1} + 0.0000141062t^{1.5} + 1.98874 \times 10^{-7}t^{2}\\
& - 4.20803 \times 10^{-9}t^{2.5} - 3.26004 \times 10^{-10}t^{3} - 8.17125 \times 10^{-12}t^{3.5} - 1.00978 \times 10^{-14}t^{4}\\
& + 6.63895 \times 10^{-15}t^{4.5} + 2.37496 \times 10^{-16}t^{5},\\
\mathscr{Z}(t) = {} & 1.14192t^{0.5} + 0.00072t^{1} + 0.0000222065t^{1.5} + 3.26438 \times 10^{-7}t^{2}\\
& - 5.953 \times 10^{-9}t^{2.5} - 4.95998 \times 10^{-10}t^{3} - 1.27614 \times 10^{-11}t^{3.5} - 2.70274 \times 10^{-14}t^{4}\\
& + 9.94454 \times 10^{-15}t^{4.5} + 3.64932 \times 10^{-16}t^{5}.
\end{aligned}$$

The HAM series up to the first ten terms when $\alpha = 0.75$ and $h = -1$ is

$$\begin{aligned}
\mathscr{S}(t) = {} & 70 - 1.24039t^{0.75} - 0.00459175t^{1.5} - 0.0000454916t^{2.25} + 1.46035 \times 10^{-6}t^{3}.\\
& + 5.8862 \times 10^{-}8t^{3.75} + 5.56212 \times 10^{-10}t^{4.5} - 1.67124 \times 10^{-11}t^{5.25} - 6.00592 \times 10^{-13}t^{6}.\\
& - 4.45029 \times 10^{-15}t^{6.75} + 1.82285 \times 10^{-16}t^{7.5},\\
\mathscr{I}(t) = {} & 2 + 0.130568t^{0.75} + 0.00370108t^{1.5} + 0.0000265559t^{2.25} - 1.56693 \times 10^{-6}t^{3}\\
& - 5.31655 \times 10^{-8}t^{3.75} - 3.89197 \times 10^{-10}t^{4.5} + 1.77771 \times 10^{-11}t^{5.25} + 5.54742 \times 10^{-13}t^{6}
\end{aligned}$$

$$+ 3.15278 \times 10^{-15} t^{6.75} - 1.88931 \times 10^{-16} t^{7.5},$$

$$\mathscr{R}(t) = 0.00870452 t^{0.75} + 0.000349045 t^{1.5} + 7.35587 \times 10^{-6} t^{2.25} + 3.88812 \times 10^{-8} t^{3} - 2.29545 \times 10^{-9} t^{3.75} - 6.59329 \times 10^{-11} t^{4.5} - 4.03462 \times 10^{-13} t^{5.25} + 1.84643 \times 10^{-14} t^{6} + 5.13787 \times 10^{-16} t^{6.75} + 2.52383 \times 10^{-18} t^{7.5},$$

$$\mathscr{Z}(t) = 1.10112 t^{0.75} + 0.000541622 t^{1.5} + 0.0000115798 t^{2.25} + 6.76979 \times 10^{-8} t^{3} - 3.40099 \times 10^{-9} t^{3.75} - 1.01081 \times 10^{-10} t^{4.5} - 6.612 \times 10^{-13} t^{5.25} + 2.73858 \times 10^{-14} t^{6} + 7.83723 \times 10^{-16} t^{6.75} + 4.12158 \times 10^{-18} t^{7.5}.$$

Additionally, the RKM and the HWT are used to resolve the above problem. Graphs and tables are used to explain the results that were obtained. Tables 1 and 2 give the values of $\mathscr{S}(t)$ for integer and noninteger values of α. The geometrical comparison of the HAM, RKM, and HTM solutions of $\mathscr{S}(t)$ is shown in Figure 1. The graphical depiction of the HAM solution with various values of α of $\mathscr{S}(t)$ is shown in Figure 2. Figure 3 displays the error analysis of the HAM, RKM, and HWT answers with the precise solution for $\mathscr{S}(t)$. Figure 4 compares the ND Solver, HAM, RKM, and HTM solutions of $\mathscr{I}(t)$ geometrically. The HAM solution is graphically depicted with various values of α of $\mathscr{I}(t)$ in Figure 5. Figure 6 depicts the error analysis of the $\mathscr{I}(t)$ solutions from the HAM, RKM, HWT, and ND Solvers. Tables 3 and 4 contain numerical values of $\mathscr{I}(t)$ for the fractional and non-fractional values of α, respectively. Figures 7, 8, and 9 show the graphical representation of solutions obtained by different methods, solutions for different values of α, and error analysis, respectively, for $\mathscr{R}(t)$, and the corresponding values are shown in Tables 5 and 6. Tables 7 and 8 display the values of $\mathscr{Z}(t)$ for integer and noninteger values of α, and their graphical representations, along with the absolute errors, are represented in Figures 10, 11, and 12. The HAM calculations were computed using Mathematica software.

Figure 13 shows the Ebola model's nature with the varying infection rate. It shows that the infected, recovered, and dead populations increase with the infection rate, whereas the susceptible population decreases as the rate of infection increases. The characteristics of the Ebola model with varying rates of natural death are illustrated in Figure 15. It demonstrates that while the susceptible, infected, and dead populations decrease as the rate of natural death rises, the recovery population grows with the rate of natural death. The characteristics of the Ebola model, with its fluctuating susceptibility rate, are seen in Figure 14. It demonstrates that while the recovery population declines as the rate of susceptible rises, the populations of the susceptible, infected, and dead grow. Figure 16 shows the nature of the Ebola model with the varying recovery rate. It shows that the infected and dead populations decrease with the increase in the rate of recovery, but the susceptible and recovered populations increase as the rate of recovery increases.

Table 1. Comparison of solutions obtained from the ND Solver, HAM, HWT, and their absolute errors (AE) with the ND Solver solution for integer order $\alpha = 1$ of $\mathscr{S}(t)$.

t	ND Solver	HAM	RKM	HWT	HAM Error	RKM Error	HWT Error
0	70	70	70	70	0	0	0
2	68.26646136	68.26646129	68.266462	68.26643796	6.2525×10^{-8}	6.4422×10^{-7}	2.34004×10^{-5}
4	66.50506092	66.50506084	66.505062	66.50503436	7.5292×10^{-8}	1.0833×10^{-6}	2.6559×10^{-5}
6	64.71477474	64.71477485	64.714776	64.71474512	1.1560×10^{-7}	1.2643×10^{-6}	2.9619×10^{-5}
8	62.89482149	62.89482161	62.894824	62.89478857	1.2259×10^{-7}	2.5095×10^{-6}	3.2923×10^{-5}
10	61.04471044	61.0447103	61.044713	61.04467394	1.3459×10^{-7}	2.5648×10^{-6}	3.6498×10^{-5}
12	59.16428922	59.16428922	59.164292	59.1642496	5.0549×10^{-9}	2.7764×10^{-6}	3.9634×10^{-5}
14	57.25379169	57.25379162	57.253795	57.2537489	7.1567×10^{-8}	3.3131×10^{-6}	4.2854×10^{-5}
16	55.31387698	55.31387695	55.313881	55.3138312	3.4054×10^{-8}	4.0206×10^{-6}	4.5792×10^{-5}
18	53.34566544	53.34566531	53.345670	53.3456169	1.3015×10^{-7}	4.5559×10^{-6}	4.8622×10^{-5}
20	51.35076296	51.3507628	51.350768	51.35071189	1.6213×10^{-7}	5.0361×10^{-6}	5.1082×10^{-5}

TABLE 2. Comparison of the HAM and HWT solutions for different fractional values of α of $\mathscr{S}(t)$.

t	$\alpha = 0.25$		$\alpha = 0.5$		$\alpha = 0.75$	
	HAM	HWT	HAM	HWT	HAM	HWT
0	70	70	70	70	70	70
2	68.86055196	68.84302153	68.61379653	68.70546622	68.4117229	68.54300974
4	68.64232277	68.53664736	68.0310697	67.97827538	67.31141932	67.35769455
6	68.49549828	68.53807154	67.58031924	67.58450622	66.33454123	66.37581115
8	68.38164118	68.37879865	67.19779941	67.20553693	65.42691749	65.465631335
10	68.28732542	68.26733001	66.85882923	66.85511223	64.56548888	64.59894303
12	68.20612471	68.22056551	66.55075585	66.55309132	63.73768115	63.76964372
14	68.13441769	68.12386092	66.26606611	66.26655202	62.93568276	62.96585806
16	68.06994401	68.07014061	65.99986673	66.00050356	62.15422837	62.18322697
18	68.01118957	68.01935681	65.74876027	65.75005799	61.38956504	61.41781415
20	67.95708612	67.90528408	65.51027414	65.50807027	60.6389079	60.66565703

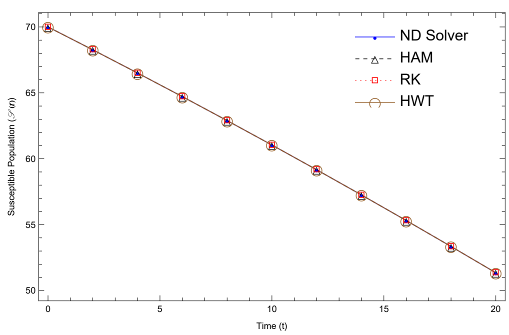

FIGURE 1. Comparison of the ND Solver solution with the HAM, RKM, and HWT solutions for $\mathscr{S}(t)$.

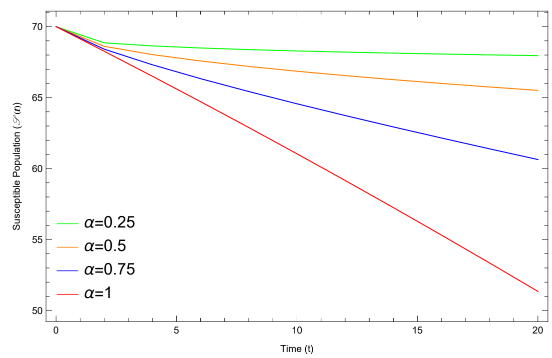

FIGURE 2. Graphical interpretation of the HAM solutions ($\mathscr{S}(t)$) at different values of α.

TABLE 3. Comparison of solutions obtained from the ND Solver, HAM, HWT, and their absolute errors (AE) with the ND Solver solution for integer order $\alpha = 1$ of $\mathscr{I}(t)$.

t	ND Solver	HAM	RKM	HWT	HAM Error	RKM Error	HWT Error
0	2	2	2	2	0	0	0.
2	2.25109815	2.25109820	2.251098	2.25111735	5.2441×10^{-8}	1.5468×10^{-7}	1.9201×10^{-5}
4	2.52488223	2.52488229	2.524882	2.52490396	6.0790×10^{-8}	2.3705×10^{-7}	2.1724×10^{-5}
6	2.82192484	2.82192470	2.821923	2.82194893	1.4058×10^{-7}	1.8413×10^{-6}	2.4089×10^{-5}
8	3.14254760	3.14254745	3.142546	3.14257425	1.5040×10^{-7}	1.6032×10^{-6}	2.6654×10^{-5}
10	3.48677874	3.48677884	3.486777	3.48680818	1.0264×10^{-7}	1.7448×10^{-6}	2.9439×10^{-5}
12	3.85431151	3.85431148	3.854309	3.85434325	2.5110×10^{-8}	$,2.5096\times10^{-6}$	3.1750×10^{-5}
14	4.24446351	4.24446355	4.244460	4.24449761	3.6707×10^{-8}	3.5153×10^{-6}	3.4099×10^{-5}
16	4.65614537	4.65614537	4.656142	4.65618151	1.1610×10^{-9}	3.3745×10^{-6}	3.6143×10^{-5}
18	5.08783327	5.08783335	5.087829	5.08787132	8.3409×10^{-8}	4.2721×10^{-6}	3.8049×10^{-5}
20	5.537553362	5.537553476	5.537549	5.53759294	1.1373×10^{-7}	4.3620×10^{-6}	3.9584×10^{-5}

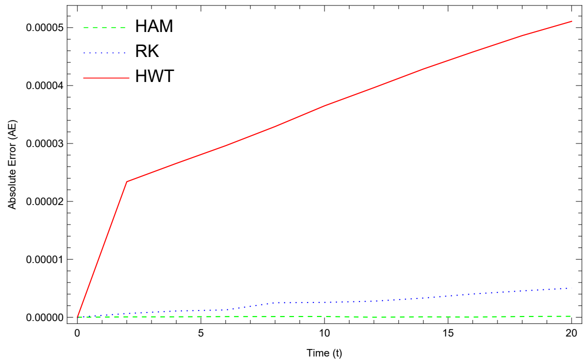

FIGURE 3. Error analysis of the HAM, RKM, and HWT solutions ($\mathscr{S}(t)$) with ND Solver solutions.

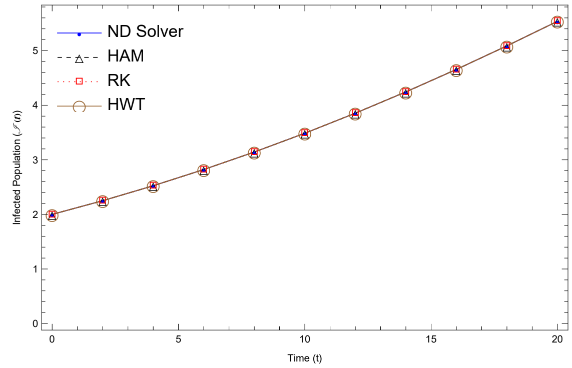

FIGURE 4. Comparison of the ND Solver solution with the HAM, RKM, and HWT solutions for $\mathscr{I}(t)$.

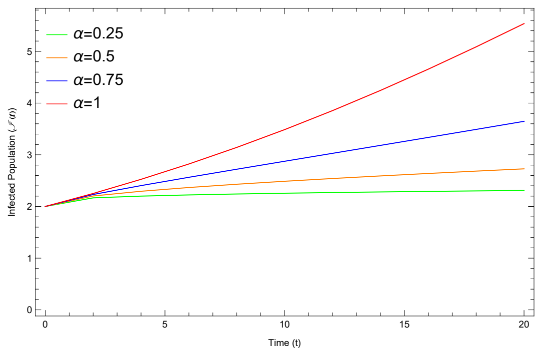

FIGURE 5. Graphical interpretation of the HAM solutions ($\mathscr{I}(t)$) at different values of α.

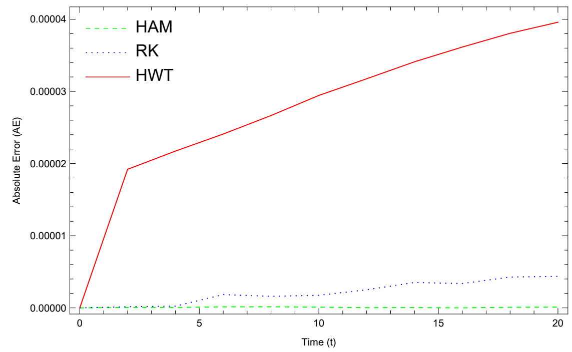

FIGURE 6. Error analysis of the HAM, RKM, and HWT solutions ($\mathscr{I}(t)$) with ND Solver solutions.

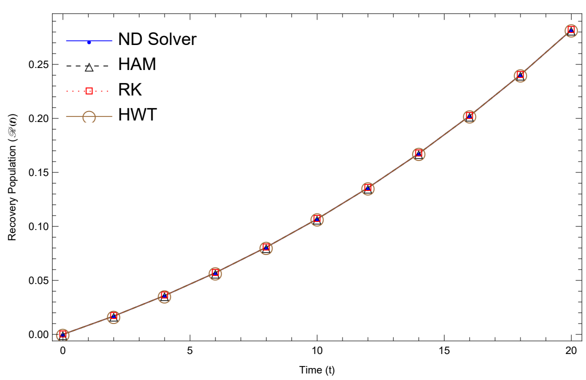

FIGURE 7. Comparison of the ND Solver solution with the HAM, RKM, and HWT solutions for $\mathscr{R}(t)$.

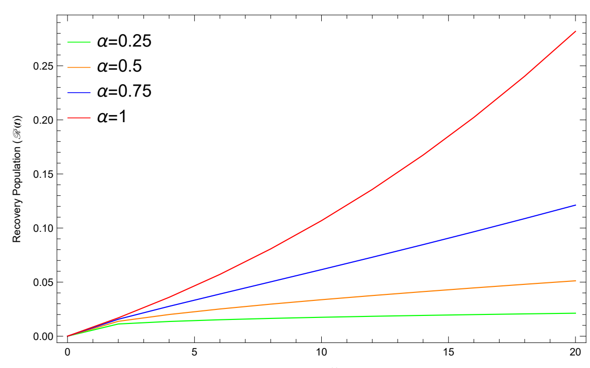

FIGURE 8. Graphical interpretation of the HAM solutions ($\mathscr{R}(t)$) at different values of α.

TABLE 4. Comparison of the HAM and HWT solutions for different fractional values of α of $\mathscr{I}(t)$.

t	$\alpha = 0.25$		$\alpha = 0.5$		$\alpha = 0.75$	
	HAM	HWT	HAM	HWT	HAM	HWT
0	2	2	2	2	2	2
2	2.16657018	2.16853444	2.20284806	2.18850253	2.23152917	2.21276099
4	2.20024690	2.21551672	2.29385435	2.29989271	2.40360184	2.39505645
6	2.22323451	2.21736755	2.36662295	2.36541825	2.56438595	2.55609728
8	2.24124477	2.24151685	2.43001482	2.42829613	2.72048580	2.71214011
10	2.25628647	2.25912787	2.48745410	2.48728226	2.87455988	2.86651325
12	2.26932594	2.26738716	2.54069282	2.53979361	3.02797377	3.01977607
14	2.28090992	2.28231297	2.59076934	2.59012382	3.18151828	3.17321800
16	2.29138085	2.29139572	2.63835862	2.63771734	3.33568181	3.32721385
18	2.30096882	2.29990688	2.68392827	2.68322173	3.49077490	3.48209625
20	2.30983661	2.31662891	2.72781802	2.72756218	3.64699463	3.63820268

TABLE 5. Comparison of solutions obtained from the ND Solver, HAM, HWT, and their absolute errors (AE) with the ND Solver solution for integer order $\alpha = 1$ of $\mathscr{R}(t)$.

t	ND Solver	HAM	RKM	HWT	HAM Error	RKM Error	HWT Error
0	0	0	0	0	0	0	0.
2	0.01695623	0.01695624	0.016956	0.01695788	3.9673×10^{-9}	2.3656×10^{-7}	1.6442×10^{-6}
4	0.03593972	0.03593973	0.035940	0.03594161	5.6905×10^{-9}	2.7299×10^{-7}	1.8914×10^{-6}
6	0.05712593	0.05712594	0.057126	0.05712809	9.4929×10^{-9}	6.2464×10^{-8}	2.1615×10^{-6}
8	0.08069324	0.08069325	0.080693	0.08069569	1.0585×10^{-8}	2.4204×10^{-7}	2.4487×10^{-6}
10	0.10682072	0.10682073	0.106821	0.10682347	1.2536×10^{-8}	2.7967×10^{-7}	2.7552×10^{-6}
12	0.13568565	0.13568566	0.135686	0.13568873	1.1649×10^{-8}	3.4348×10^{-7}	3.0752×10^{-6}
14	0.16746069	0.16746070	0.167461	0.16746410	1.3551×10^{-8}	3.0794×10^{-7}	3.4117×10^{-6}
16	0.20231073	0.20231075	0.202311	0.20231449	1.3619×10^{-8}	2.6342×10^{-7}	3.7569×10^{-6}
18	0.24038961	0.24038962	0.240389	0.24039372	1.8244×10^{-8}	6.1148×10^{-7}	4.1134×10^{-6}
20	0.28183658	0.28183660	0.281836	0.28184105	1.8872×10^{-8}	5.8263×10^{-7}	4.4689×10^{-6}

TABLE 6. Comparison of the HAM and HWT solutions for different fractional values of α of $\mathscr{R}(t)$.

t	$\alpha = 0.25$		$\alpha = 0.5$		$\alpha = 0.75$	
	HAM	HWT	HAM	HWT	HAM	HWT
0	0	0	0	0	0	0
2	0.01127650	0.01139717	0.01374021	0.01274621	0.01566637	0.01440047
4	0.01359692	0.01462846	0.02004201	0.02041390	0.02760471	0.02697983
6	0.01518844	0.01479964	0.02514037	0.02504810	0.03898377	0.03836340
8	0.01643963	0.01645463	0.02962416	0.02949592	0.05023647	0.04959877
10	0.01748744	0.01767844	0.03372060	0.03369383	0.06154038	0.06090756
12	0.01839787	0.01827097	0.03754579	0.03747386	0.07299020	0.07233326
14	0.01920829	0.01929986	0.04116844	0.04111295	0.08464408	0.08396548
16	0.01994216	0.01994457	0.04463317	0.04457857	0.09654113	0.09583609
18	0.02061522	0.02054685	0.04797084	0.04791257	0.10870933	0.10797443
20	0.02123865	0.02167831	0.05120384	0.05117410	0.12116961	0.12041016

TABLE 7. Comparison of solutions obtained from the ND Solver, HAM, HWT, and their absolute errors (AE) with the ND Solver solution for integer order $\alpha = 1$ of $\mathscr{X}(t)$.

t	ND Solver	HAM	RKM	HWT	HAM Error	RKMError	HWT Error
0	0.	0.	0	0	0	0	0.
2	1.46548425	1.46548425	1.465484	1.46548681	6.1166×10^{-9}	2.5297×10^{-7}	2.5548×10^{-6}
4	2.93411711	2.93411712	2.934117	2.93412006	8.8114×10^{-9}	1.1929×10^{-7}	2.9427×10^{-6}
6	4.40617448	4.40617450	4.406174	4.40617785	1.5491×10^{-8}	4.8538×10^{-7}	3.3679×10^{-6}
8	5.88193766	5.88193768	5.881938	5.88194148	1.7226×10^{-8}	3.3571×10^{-7}	3.8202×10^{-6}
10	7.36169010	7.36169011	7.361690	7.36169440	1.9410×10^{-8}	9.9704×10^{-8}	4.3028×10^{-6}
12	8.84571361	8.84571362	8.845713	8.84571841	1.8521×10^{-8}	6.1031×10^{-7}	4.8093×10^{-6}
14	10.33428411	10.33428413	10.334284	10.33428944	2.1316×10^{-8}	1.0565×10^{-7}	5.3424×10^{-6}
16	11.82766691	11.82766693	11.827667	11.82767280	2.1597×10^{-8}	9.0502×10^{-8}	5.8914×10^{-6}
18	13.32611167	13.32611170	13.326111	13.32611813	2.8483×10^{-8}	6.7230×10^{-7}	6.4598×10^{-6}
20	14.82984709	14.82984712	14.829847	14.82985412	2.9522×10^{-8}	9.1470×10^{-8}	7.0293×10^{-6}

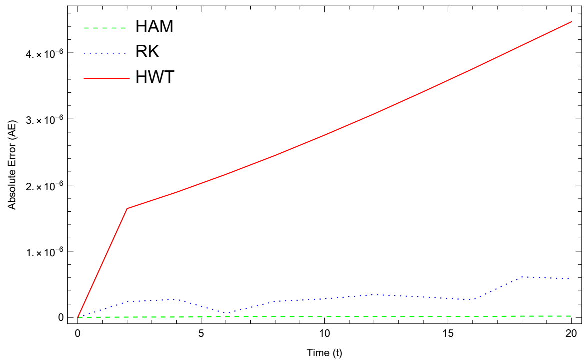

FIGURE 9. Error analysis of the HAM, RKM, and HWT solutions ($\mathscr{R}(t)$) with ND Solver solutions.

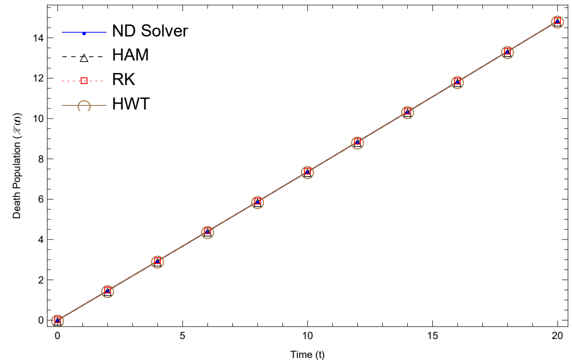

FIGURE 10. Comparison of the ND Solver solution with the HAM, RKM, and HWT solutions for $\mathscr{Z}(t)$.

TABLE 8. Comparison of the HAM and HWT solutions for different fractional values of α of $\mathscr{Z}(t)$.

t	$\alpha = 0.25$		$\alpha = 0.5$		$\alpha = 0.75$	
	HAM	HWT	HAM	HWT	HAM	HWT
0	0	0	0	0	0	0
2	0.96160134	0.97704683	1.16961518	1.09328504	1.34108155	1.22982879
4	1.14383338	1.23320743	1.65503392	1.70141798	2.25737411	2.22026914
6	1.26607875	1.22976124	2.02791743	2.02502740	3.06208904	3.02972814
8	1.36067441	1.36322985	2.34256160	2.33667100	3.80236023	3.77262978
10	1.43890065	1.45586369	2.61999609	2.62391160	4.498410848	4.4736361
12	1.50615147	1.49377634	2.87100554	2.86964120	5.16135487	5.13824693
14	1.56546408	1.57452621	3.10199610	3.10221119	5.79815487	5.77695843
16	1.61873297	1.61851908	3.31714149	3.31720051	6.41354867	6.39372307
18	1.66722637	1.66018944	3.51934061	3.51880769	7.01095071	6.99211515
20	1.71183860	1.75640868	3.71070399	3.71319343	7.59292784	7.57573011

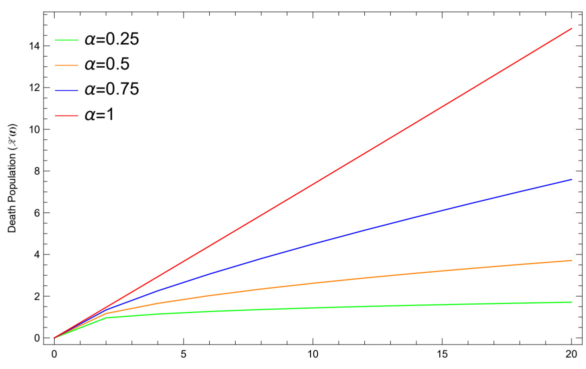

FIGURE 11. Graphical interpretation of the HAM solutions $\mathscr{Z}(t)$ at different values of α.

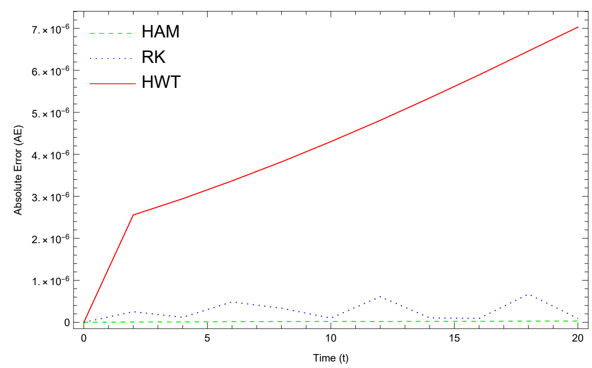

FIGURE 12. Error analysis of the HAM, RKM, and HWT solutions ($\mathscr{Z}(t)$) with ND Solver solutions.

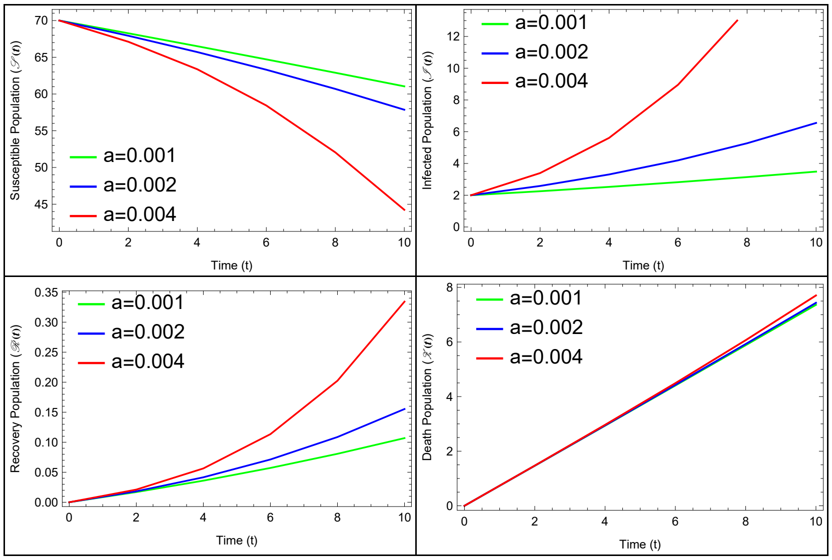

FIGURE 13. The nature of the model with the increase in the rate of infection (a).

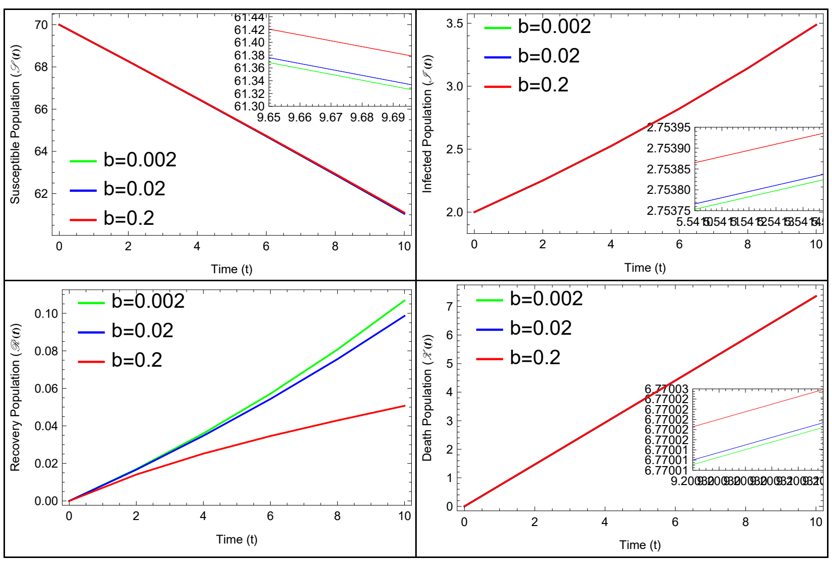

FIGURE 14. The nature of the model with the increase in the rate of susceptibility (b).

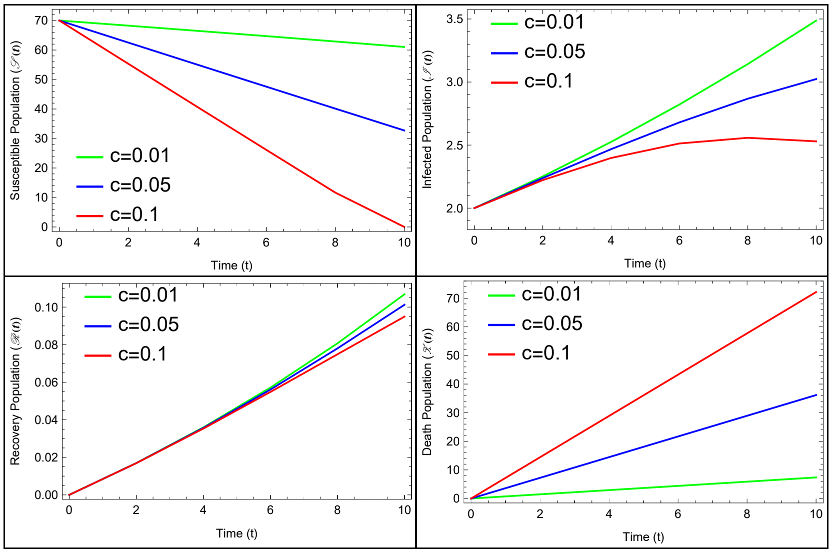

FIGURE 15. The nature of the model with the increase in the rate of natural death (c).

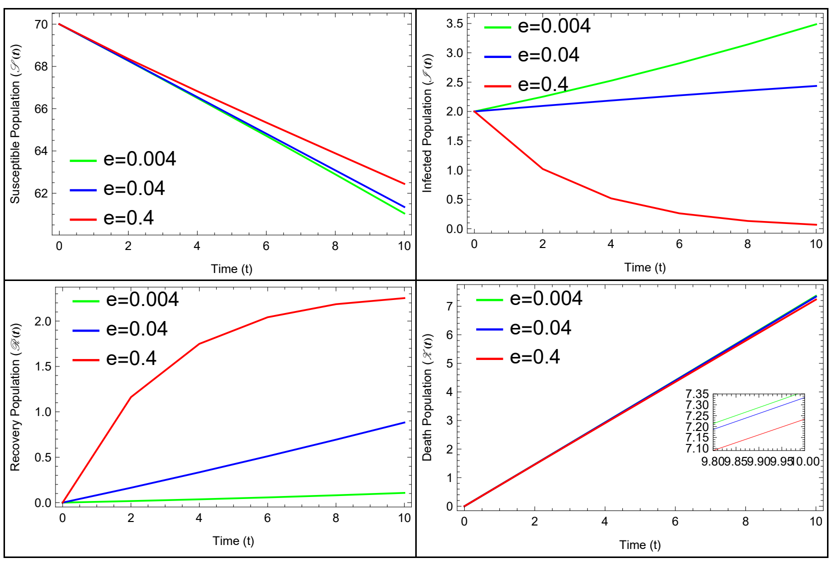

FIGURE 16. The nature of the model with the increase in the rate of recovery (e).

6. Conclusion

In this study, we discussed the Ebola virus model through three different methods, such as the homotopy analysis method, the Haar wavelet technique, and the Runge-Kutta method. Here, we numerically analyzed susceptible, infected, recovery, and dead populations and discussed the effect of different parameters. The homotopy analysis method is a semi-analytical method that yields the analytical solution of a given model after some more deformations. The Haar wavelet method is a numerical technique that solves the models numerically with the help of software. The obtained solutions are numerically tabulated in Tables 1-8. Figures 1-12 show the performance of the methods, and Figures 13-16 show the nature of the model with varying parameters. Here, the HAM consumes more time to yield solutions for the different models. Still, the HWT delivers the numerical results with less time, and the results are compared with the ND Solver and Runge-Kutta method solutions. This study reveals that the HAM provides solutions with high accuracy compared to other methods.

Acknowledgment

Authors are grateful to their anonymous referees and editor for their constructive comments.

References

[1] A. Atangana and E. F. Goufo, *On the mathematical analysis of Ebola hemorrhagic fever: deathly infection disease in West African countries*, BioMed research international, *2014*(1) (2014), 261383.

[2] A. Atangana and K. M. Owolabi, *New numerical approach for fractional differential equations*, Mathematical Modelling of Natural Phenomena, *13*(1) (2018), 3.

[3] Y. Chen, M. Yi, and C. Yu, *Error analysis for numerical solution of fractional differential equation by Haar wavelets method,* Journal of Computational Science, *3*(5) (2012), 367-73.

[4] M. H. Derakhshan, *The stability analysis and numerical simulation based on Sinc Legendre collocation method for solving a fractional epidemiological model of the Ebola virus*, Partial Differential Equations in Applied Mathematics, *3* (2021), 100037.

[5] M. A. Dokuyucu and H. Dutta, *A fractional order model for Ebola Virus with the new Caputo fractional derivative without singular kernel,* Chaos, Solitons & Fractals, *134* (2020), 109717.

[6] O. Ilhan and G. Şahin, *A numerical approach for an epidemic SIR model via Morgan-Voyce series,* International Journal of Mathematics and Computer in Engineering, (2024).

[7] H. Jafari, P. Goswami, R. S. Dubey, S. Sharma, and A. Chaudhary, *Fractional SIZR model of Zombies infection*, International Journal of Mathematics and Computer in Engineering, (2023).

[8] F. M. Khan, A. Ali, E. Bonyah, and Z. U. Khan, [Retracted] *The Mathematical Analysis of the New Fractional Order Ebola Model*, Journal of Nanomaterials, *2022*(1) (2022), 4912859.

[9] S. Kumbinarasaiah, *A novel approach for multi dimensional fractional coupled Navier–Stokes equation,* SeMA Journal, *80*(2) (2023), 261-282.

[10] S. Kumbinarasaiah and M. P. Preetham, *A study on homotopy analysis method and clique polynomial method,* Computational Methods for Differential Equations, *10*(3) (2022) 774-88.

[11] S. Kumbinarasaiah and M. Mulimani, *The Fibonacci wavelets approach for the fractional Rosenau–Hyman equations*, Results in Control and Optimization, *1* (2023), 100221.

[12] S. Kumbinarasaiah and R. A. Mundewadi, *Numerical solution of fractional-order integro-differential equations using Laguerre wavelet method,* Journal of Information and Optimization Sciences, *43*(4) (2022), 643-662.

[13] S. Liang and D. J. Jeffrey, *Comparison of homotopy analysis method and homotopy perturbation method through an evolution equation*, Communications in Nonlinear Science and Numerical Simulation, *14*(12) (2009),4057-64.

[14] S. Liao, *On the proposed homotopy analysis technique for nonlinear problems and its applications*, Shanghai Jiao Tong University, (1992).

[15] S. Liao, *An explicit, totally analytic approximate solution for Blasius' viscous flow problems*, International Journal of Non-Linear Mechanics, *34*(4) (1999),759-78.

[16] S. Liao, *Beyond perturbation: introduction to the homotopy analysis method,* Chapman and Hall/CRC, 2003.

[17] S. Liao , *Homotopy analysis method in nonlinear differential equations,* Beijing: Higher education press, (2012).

[18] S. Liao, *Advances in the homotopy analysis method,* World Scientific, (2013).

[19] Z. M. Odibat, *A study on the convergence of homotopy analysis method,* Applied Mathematics and Computation, *217*(2) (2010), 782-789.

[20] A. Rachah and D. F. M. Torres, *Predicting and controlling the Ebola infection,* Mathematical Methods in the Applied Sciences, *40*(17) (2017), 6155-6164.

[21] S. Rewar and D. Mirdha, *Transmission of Ebola virus disease: an overview,* Annals of global health, *80*(6) (2014), 444-451.

[22] Z. Sabir and M. Umar, *Levenberg-Marquardt backpropagation neural network procedures for the consumption of hard water-based kidney function,* International Journal of Mathematics and Computer in Engineering, *1*(1) (2023), 127-138.

[23] M. Sajid and T. Hayat, *Comparison of HAM and HPM methods in nonlinear heat conduction and convection equations,* Nonlinear Analysis: Real World Applications, *9*(5) (2008), 2296-2301.

[24] S. C. Shiralasetti and S. Kumbinarasaiah, *Some results on Haar wavelets matrix through linear algebra,* Wavelet and Linear Algebra, *4*(2) (2017), 49-59.

[25] H. Singh, *Analysis for fractional dynamics of Ebola virus model,* Chaos, Solitons & Fractals, *138* (2020), 109992.

[26] K. Srinivasa, H. M. Baskonus, and Y. G. Sánchez, *Numerical solutions of the mathematical models on the digestive system and covid-19 pandemic by hermite wavelet technique,* Symmetry, *13*(12) (2021), 2428.

[27] H. M. Srivastava and M. S. Khaled, *Numerical simulation of the fractal-fractional Ebola virus,* Fractal and Fractional, *4*(4) (2020), 49.

[28] H. M. Srivastava, M. S. Khaled, and M. M. Khader, *An efficient spectral collocation method for the dynamic simulation of the fractional epidemiological model of the Ebola virus,* Chaos, Solitons & Fractals, *140* (2020), 110174.

[29] H. M. Srivastava and S. Deniz, *A new modified semi-analytical technique for a fractional-order Ebola virus disease model* Revista de la Real Academia de Ciencias Exactas, Físicas Naturales Serie A, Matemáticas, *115*(3) (2021), 137.

[30] M. Zurigat, S. Momani, Z. Odibat, and A. Alawneh, *The homotopy analysis method for handling systems of fractional differential equations,* Applied Mathematical Modelling, *34*(1) (2010), 24-35.